Nuclear Science and Techniques (2026) 37:131
https://doi.org/10.1007/s41365-026-01924-3

Prompt fission neutron uranium logging (III): logging instrument

Hai-Tao Wang[1,2] · Yan Zhang[1,2] · Chi Liu[1,2] · Jian-Qiang Xu[1,2] · Li-Jiao Zhang[1,2] · Zhi-Feng Liu[1,2] · Xiong-Jie Zhang[1,2] · Rui Chen[1,2] · Qi Liu[1,2] · Ren-Bo Wang[1,2] · Shu-Min Zhou[1,2] · Bin Tang[1,2]

Received: 10 October 2024 / Revised: 16 December 2024 / Accepted: 25 December 2024 / Published online: 29 April 2026

Abstract

The domestically developed prompt fission neutron uranium logging (PFNUL) instrument for uranium exploration represents a significant advancement in China's deep uranium mining efforts, although it has considerable challenges and complexity. This paper presents the development of a new prompt fission neutron uranium logging instrument (named UNL4) that integrates a domestic D-T neutron generator, two ^{3}He proportional detectors, a lanthanum bromide ($LaBr_3$) gamma-ray detector, and a digital multi-channel pulse amplitude analyzer. The near ^{3}He detector is shielded with 1 mm of cadmium (Cd) and 5 mm of high-density polyethylene (HDPE), enabling efficient epithermal neutron detection, whereas the far ^{3}He detector measures thermal neutrons. A $LaBr_3$ detector is employed for gamma-ray detection, primarily originating from uranium decay. High-speed analog-to-digital converter (ADC) and field-programmable gate array (FPGA) technologies are used to achieve rapid acquisition and transmission of both dual-energy neutron time spectra and gamma spectra. Moreover, this paper proposes a fast signal-shaping method, which reduces the dead time effect in ^{3}He detectors on neutron time spectra. Experiments conducted in standard model boreholes with varying uranium contents demonstrated a strong linear relationship between the epithermal-to-thermal neutron ratio (*E*/*T*) and uranium content, with a fitting coefficient of $R^2 > 0.999$, confirming the accuracy of the instrument. The *E*/*T* value repeatability, in both short-term (3.16% *RSD*) and long-term (1.2% *RSD*) measurements, showed excellent stability. In addition, the instrument demonstrated good performance at neutron-logging speeds of $0.3 \sim 3\,\mathrm{m/min}$ (*E*/*T* values) and gamma logging speeds of $1 \sim 10\,\mathrm{m/min}$. Through measurements in two ore sections of the PU model with uranium contents of 87.1 ppm and 45.6 ppm showed that *RD* remained below approximately 10% at logging speeds of 0–2 m/s in both cases, satisfying the requirements for engineering applications. This marks the first successful development of a neutron-logging instrument for uranium exploration based on a domestic neutron generator and signifies an important contribution to uranium resource exploration.

Keywords Uranium exploration · Neutron-logging instrument · Pulsed neutron · Neutron time spectrum detection

1 Introduction

Nuclear power is one of the most promising methods for the efficient and sustainable large-scale production of hydrogen without the emission of carbon dioxide. Uranium ore, the primary fuel source for nuclear energy generation, is crucial to the development of the nuclear power industry. Since the beginning of the twenty-first century, countries worldwide have initiated mineral exploration efforts and developed intelligent technologies and equipment for mineral exploration and development, providing technological support for energy conservation and emission reduction [1–4].

The uranium logging method based on pulsed neutron technology enables the direct measurement of uranium (^{235}U) content without requiring core sampling, and it is

This work was supported by the National Natural Science Foundation of China (No. 42374226), Jiangxi Provincial Natural Science Foundation (Nos. 20232BCJ23006, gpyc20240073, 20252BAC240173 and 20243BCE51132), National Key Laboratory of Uranium Resource Exploration-Mining and Nuclear Remote Sensing (2024QZ-TD-09, 2024HDX10, 2025QZ018).

✉ Yan Zhang
yanzhang@ecut.edu.cn

1 National Key Laboratory of Uranium Resources Exploration-Mining and Nuclear Remote Sensing, East China University of Technology, Nanchang 330000, China

2 Engineering Research Center of Nuclear Technology Application, Ministry of Education, East China University of Technology, Nanchang 330013, China

not affected by gamma rays from other radioactive nuclides such as thorium and potassium [5–7]. Since the 1970s, countries such as the USA, Canada, Germany, and the former Soviet Union have conducted research and experiments on neutron-logging techniques for direct uranium measurement. Collecting neutron time spectra is widely recognized as an effective method for quantifying uranium [8–10]. However, neutron sources with ultrashort pulse widths and high yields should be used, such as the pulsed neutron uranium logging system ANHK-60 developed by the All-Russian Institute of Automated Design (VNIIA), which employs a D-T neutron generator with a pulse width of 1 μs and a single pulse yield of approximately 1×10^8 n/pulse. However, its operational life span is limited to only 150 h [11, 12].

In recent years, research on neutron logging has primarily focused on methods, theory, and simulation studies, with few reports on related instruments [13, 14]. This is largely because of the significant challenges involved in the development of uranium logging instruments. A key requirement is the use of compact neutron emitters that produce ultrashort pulses (of the order of microseconds) with high neutron yields. Currently, only a few countries, including Russia, the USA, and France, have developed this technology. Examples include the Russian ING-10-20-120 model D-T neutron emitter, French Genie 16NG, and US RTNS-II and P383 systems [15–17]. Another challenge is detecting and collecting the neutron signals generated by these short-pulse high-yield neutron sources. A widely adopted approach involves the use of high-efficiency ^{3}He proportional counters to detect epithermal or thermal neutrons. Epithermal neutron detectors are used to detect prompt neutrons produced by uranium fission, which are essential for uranium quantification [18]. For example, the Russian ANHK-60 logging instrument includes six Geiger–Müller tubes to detect gamma rays from lead and boron, forming a monitoring system for the neutron source yield, thus mitigating the impact of source flux fluctuations. The US PFN system is equipped with six miniature ^{3}He proportional counters to achieve similar functionality [19]. Over the past decade, the author team has conducted extensive research in the field of neutron logging for uranium. Through both theoretical and experimental research, they proposed a method based on the ratio of epithermal neutrons (E) to thermal neutrons (T), referred to as "E/T" [20–23]. This method is not affected by fluctuations in the neutron source yield, enabling an extended operational life span of the neutron source. Therefore, the uranium logging instrument discussed in this paper utilizes two ^{3}He proportional counters. The first, located closer to the source, is wrapped in cadmium and high-density polyethylene (HDPE) for epithermal neutron detection, whereas the second, located farther from the source, detects thermal neutrons [24–26]. However, factors such as the gas pressure and material and size of the wrapping layers significantly affect the neutron detection efficiency, which is a key topic of this study. Because the smallest exploration boreholes are only 9 cm in diameter, existing commercial multi-channel analyzers for time and energy spectra do not satisfy the size requirements for logging instruments, and the large data volumes generated require redesign and customization. This paper proposes the use of high-speed analog-to-digital converter (ADC) and field-programmable gate array FPGA technologies to enable the rapid acquisition and transmission of dual-energy neutron time spectra, combined with pulse-shaping techniques and time-spectrum processing algorithms, to satisfy the specific requirements of logging instrumentation [27].

Finally, a series of experiments was conducted using the independently developed prompt fission neutron uranium logging instrument (UNL4) in five standard model boreholes at the Nuclear Industry Airborne Survey and Remote Sensing Center. The calibration results from these model boreholes with varying uranium concentration demonstrated a strong linear relationship in the uranium content calibration equation, comparable to that obtained using a probe equipped with a Russian neutron tube. The instrument also performed well in both short- and long-term repeatability tests conducted in the same model boreholes, ensuring accurate calibration of the uranium content. A comparison of logging curves at different speeds indicated that the measurement performance is satisfactory at neutron-logging speeds ranging from 0.3 to 3 m/min and gamma logging speeds from 1 to 10 m/min. This instrument fills a critical gap in the independent development of neutron-logging instruments for uranium exploration in China and is significant to uranium resource exploration and the country's energy security.

2 Instruments and experiments

2.1 Logging instrument

The uranium logging instrument developed by our team, as shown in Fig. 1, comprises three main components: (1) a neutron source, including a D-T neutron tube and neutron emitter; (2) a detection unit featuring two ^{3}He neutron detectors and a gamma detector; and (3) an electronics unit consisting of a digital multi-channel pulse amplitude analyzer.

The D-T neutron sources used in the experiments primarily include the Russian ING-10-20-120 and FH-G5DT models from Fan-Hua Testing Technology Co., Ltd., with the detailed parameters listed in Table 1. These sources are primarily used to emit pulsed neutrons. The ^{3}He neutron detectors, also provided by Fan-Hua Testing Technology Co., Ltd., are referred to as the near ^{3}He detector and far ^{3}He detector, based on their proximity to the neutron source. The near ^{3}He detector is wrapped in Cd

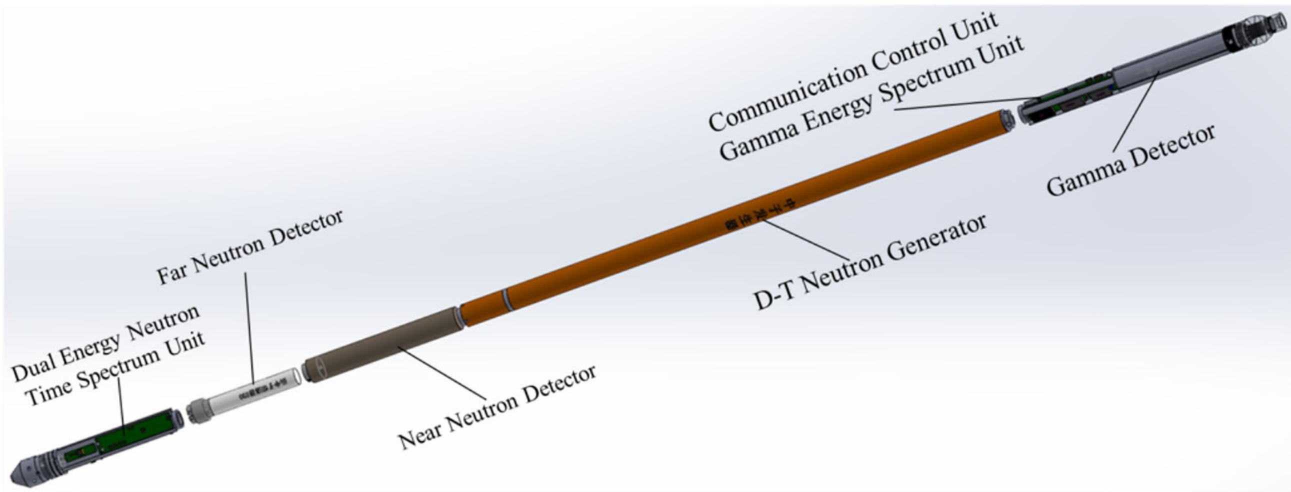

Fig. 1 (Color online) Independently developed Prompt Fission Neutron Uranium Logging Instrument (UNL4)

Table 1 D-T neutron generator parameters

Parameter	Neutron tube	
	ING-10-20-120	FH-G5DT
Neutron yield (n/s)	1.5×10^8	1×10^8
Pulse frequency (Hz)	1 ~ 20	0 ~ 1000
Life (h)	150	≥ 500
Supply voltage (V)	+150 (DC)	220 (AC/50 Hz) /48~260 (DC)
Maximum power (W)	30	50
Maximum working Temperature (°C)	+120	+150
Dimensions (mm)	Φ34 × 1300	Φ50 × 1300

metal, and a HDPE was designed to detect epithermal neutrons, whereas the far ^{3}He detector is used to detect thermal neutrons in the borehole. The gamma detector employed is a lanthanum bromide ($LaBr_3$) detector positioned at a greater distance from the neutron source to minimize the effects of gamma rays produced by neutron activation. The primary function of the $LaBr_3$ detector is to detect the natural gamma radiation emitted by the uranium ore, thereby providing an initial estimate of the ore layer's location [28]. The electronics unit consists of time and energy spectrum acquisition components. It utilizes a fully digital design that incorporates high-speed ADC, FPGA, and digital signal processing (DSP) technologies. This setup enables high-speed sampling of neutron and gamma-ray signals and intelligent processing of dual-energy neutron time and gamma spectra. The system can operate both independently and in coordinated synchronization, thereby offering enhanced performance. Further details are provided in the following sections.

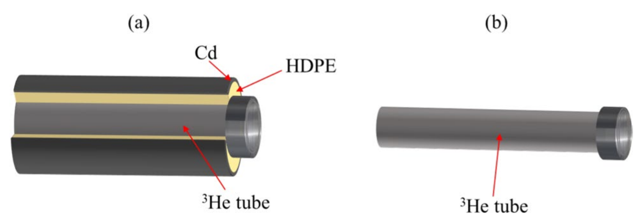

Fig. 2 (Color online) **a** Schematic of the epithermal neutron detector. **b** Schematic of the thermal neutron detector

2.2 Epithermal and thermal neutron detection

^{3}He gas detectors are commonly used for thermal neutron detection, owing to their high efficiency in capturing thermal neutrons. However, fast neutrons with energies ranging from 0 to 3 MeV are generated during uranium fission reactions. These fast neutrons are then slowed down within the formation and become epithermal neutrons. Uranium content can be estimated by detecting the number of epithermal neutrons. In oil well logging, ^{3}He gas detectors are often encased in Cd metal and a moderating material such as HDPE to detect epithermal neutrons, as shown in Fig. 2. The Cd metal absorbs thermal neutrons from the borehole, preventing their contribution to the measurement, whereas the moderating material further slows down epithermal neutrons into thermal neutrons, thus enhancing the detection efficiency.

Using the Monte Carlo simulation method, we simulated the thicknesses of the Cd metal and moderating material (HDPE) for the aforementioned epithermal neutron detector. The results are presented in Fig. 3.

Figure 3a shows that as the thickness of the Cd increased, the shielding efficiency of the epithermal

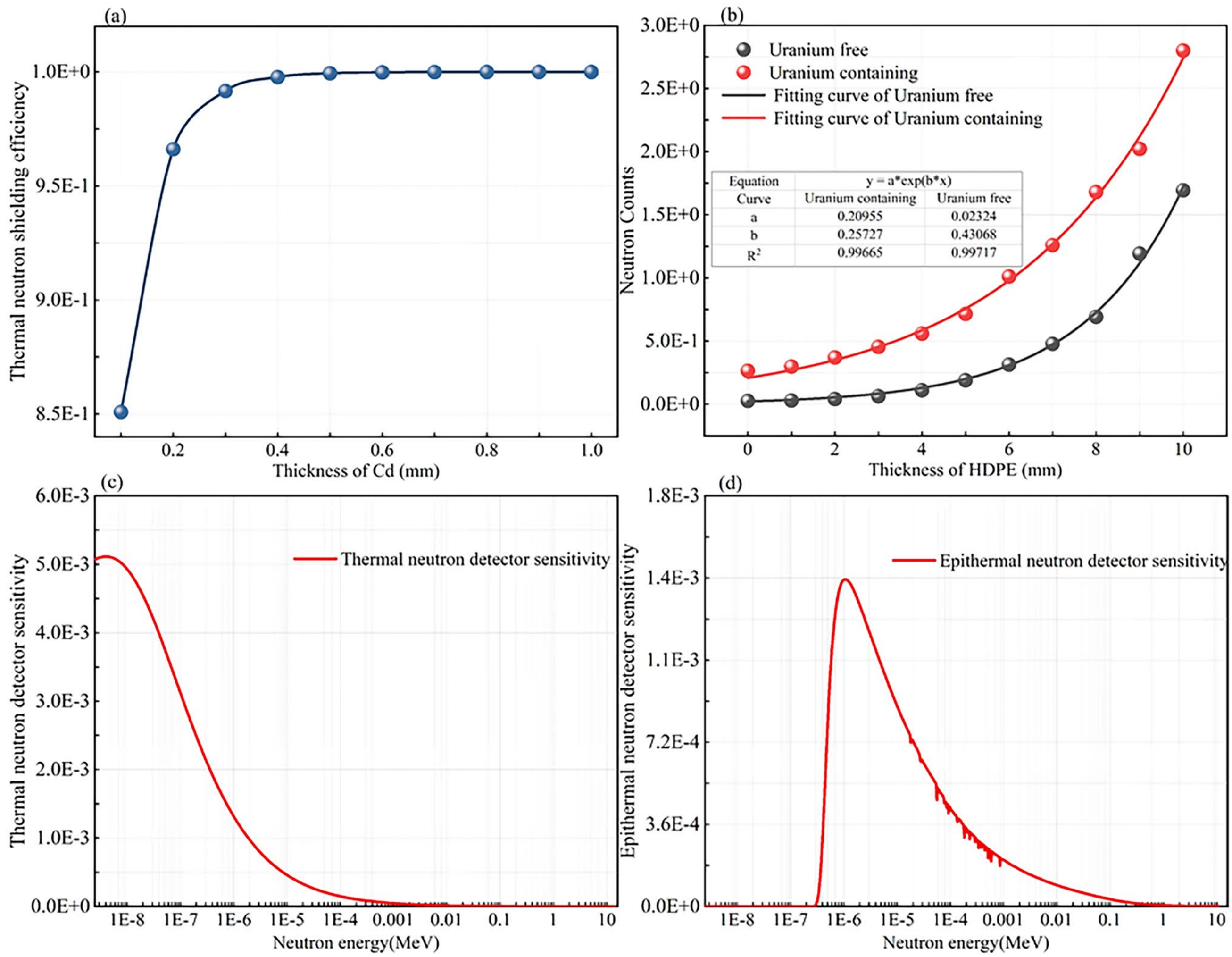

Fig. 3 (Color online) **a** Cd metal thermal neutron shielding efficiency. **b** HDPE thickness effect on epithermal neutron counting. **c** Sensitivities of the ^{3}He detector. **d** Sensitivities of the epithermal neutron detector

neutron detector for thermal neutrons increased rapidly. When the Cd thickness reached 1 mm, the shielding efficiency reached 100%, effectively blocking the thermal neutrons. Consequently, the thickness of Cd metal in the epithermal neutron detector was set to 1 mm. Figure 3b shows that as the thickness of the polyethylene increased, the counts of epithermal neutrons detected by the detector in both the uranium-free (background) and uranium-containing formations also increased. This indicated that the added layer of HDPE slows down not only the source neutrons but also the neutrons produced by uranium fission. Therefore, the counts included both epithermal neutrons generated by uranium fission and those produced by the D-T neutron generator. Considering the spatial constraints of the detector probe and other factors, the thickness of the HDPE layer was determined to be 5 mm. The final specifications and parameters of the epithermal and thermal neutron detectors are listed in Table 2.

Table 2 Specifications of each component of the epithermal and thermal neutron detector (1 atm = 101.325 kPa)

Detector	Component	Gas pressure (atm)	Density (g/cm^3)	Optimal dimension
Near detector	^{3}He detector	6	-	Φ38 mm × 150 mm
	Cd layer	-	8.65	1 mm thick
	HDPE layer	-	0.94	5 mm thick
Far detector	^{3}He detector	4	-	Φ38 mm × 150 mm

Subsequently, the detection sensitivities of the thermal and epithermal neutron detectors of different energies (ranging from 0.001 eV to 10 MeV) were calculated using Monte Carlo simulations. The sensitivity results are shown in Fig. 3. As illustrated in Fig. 3c, the thermal neutron detector exhibited a high sensitivity within the low-energy neutron range, with a rapid decrease in sensitivity as the neutron energy increased. Figure 3d shows that the designed epithermal neutron detector was more sensitive to epithermal neutrons, whereas its sensitivity to low-energy and fast neutrons was relatively low. The simulation results confirmed that the parameters determined for the epithermal and thermal neutron detectors effectively measured the formation of thermal and epithermal neutrons produced by uranium fission.

2.3 FPGA-based digital circuitry

The dual-energy neutron time-spectrum measurement unit designed for the project primarily consists of the following components: dual-energy neutron detectors and their high-voltage driving module, a preamplifier circuit, shaping amplifier circuit, polarity conversion circuit, baseline restoration circuit, signal discrimination circuit, pulse counting unit, and data analysis and communication modules. The detailed circuit structure is shown in the block diagram shown in Fig. 4.

A digital FPGA chip (radiation-resistant M2S010 from ACTEL) was selected as the core component to enable pulse counting for both epithermal and thermal neutrons while also generating the corresponding time-spectrum curves. Upon receiving a synchronized measurement signal from the pulsed neutron generator, the FPGA starts counting the pulse signals from the epithermal and thermal neutron detectors. The counts for both detectors are accumulated using a fine time-channel width of 2 μs, thus achieving a precise dual-energy neutron time-spectrum acquisition. The system simultaneously collects the neutron energy and time spectra. By analyzing the shape of the neutron energy spectrum curve, a threshold is set for the countable neutron pulses, which ensures that the time spectrum only includes valid neutron pulses, excluding noise and preventing the loss of effective neutron counts. This method ensures high accuracy in both neutron energy and time-spectrum measurements. When traditional logging systems based on analog signals are applied to uranium logging, the presence of numerous analog components, such as resistors, capacitors, and operational amplifiers, makes them highly susceptible to temperature fluctuations in downhole environments. This leads to significant temperature drift, which increases the complexity of the subsequent spectral interpretation. In contrast, the use of a high-speed digital measurement system with key components such as high-speed ADCs, FPGAs, and DSP mitigates these problems. In this system, the radiation pulse signal output of the detector is amplified and directly sampled in full pulse form using a high-speed ADC (with a sampling rate of 60 MHz and precision of 12 bits/1 V). This approach captures the entire pulse waveform rather than only the peak value, as is the case in traditional systems. Algorithms such as digital filtering and pulse shaping (using a dynamic trapezoidal shaping algorithm with adjustable parameters) are implemented using the FPGA's internal programmable digital circuits. This enables peak extraction, identification, and separation of pileup pulses and the generation of the energy spectrum curve. More complex tasks, such as the dynamic temperature correction of pulse amplitudes and communication processing, are handled by the DSP. The designed digital measurement system includes a detector, preamplifier circuit, signal conditioning circuit,

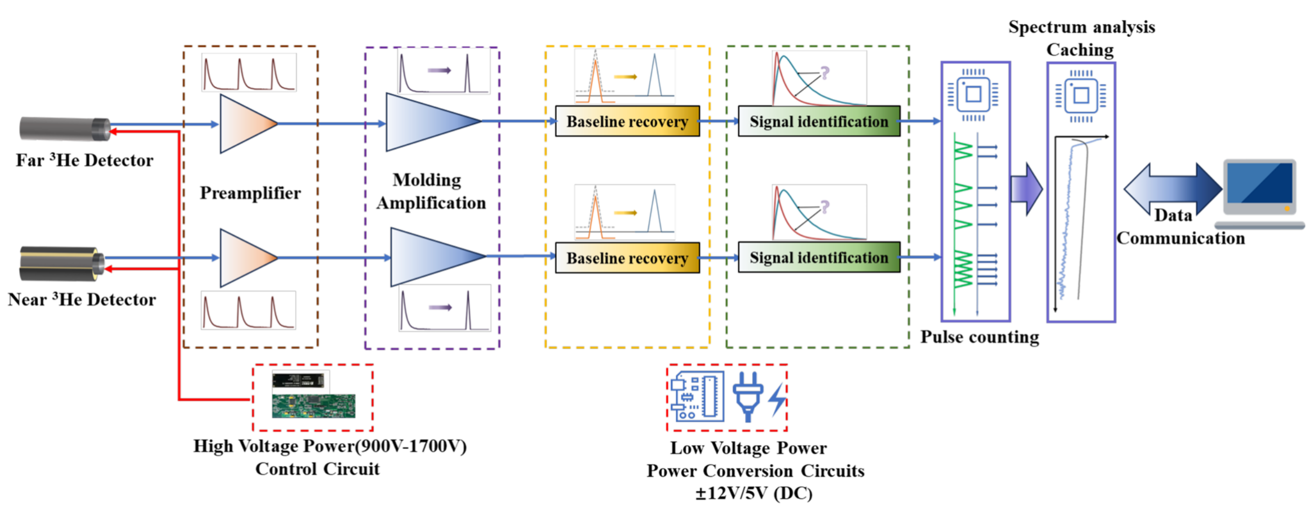

Fig. 4 (Color online) Block diagram of dual-energy neutron time-spectrum measurement circuit structure

high-speed ADC, FPGA, and DSP. The influence of the power noise ripple and other electronic interferences on the energy spectrum is controlled to $\leq 5\ \mathrm{mV}/1\ \mathrm{V}$, meaning that for a 1024-channel energy spectrum, noise contributes to no more than five channels.

2.4 Pulse fast shaping neutron time spectrum

In a dual-energy neutron time-spectrum detection system, a key challenge results because of the high neutron count rate detected by the neutron detectors immediately after the neutron pulse is emitted by the neutron source. This can cause significant pulse pileup, particularly when using standard charge-sensitive preamplifier circuits paired with ^{3}He proportional counters, which have prolonged tail times for signal decay. This pileup effect often leads to the saturation of the counting rate. To address this problem, a charge-sensitive preamplifier circuit based on narrow pulse shaping was designed for the neutron detector, which significantly improved the pulse throughput of the neutron signals. Additionally, the electronics system incorporates full-pulse high-speed sampling technology, in which the raw input pulse signals are directly sampled by a high-speed ADC, providing a complete waveform of the radiation pulse. The programmable digital circuits inside the FPGA implement triangular shaping algorithms, enabling the development of a dual-energy neutron time-spectrum measurement system for PFNUL under high count rates. This narrow pulse-shaping technique allows the processing of wider detector pulses into narrower pulses, facilitating counting measurements at high pulse throughputs [29–31]. The shaped pulse width is adjustable, and the experimental results, shown in Fig. 5a, demonstrate a reduction in signal pulse width from 1 µs to 300 ns. This enhancement increases the pulse processing capability of the electronic system from 100 kcps to over 330 kcps, ensuring the validity of count measurements under high-count-rate conditions. After processing using the anti-saturation neutron detection system, the time spectra before and after fast shaping were obtained using the logging model for practical testing, as shown in Fig. 5b.

Additionally, the project conducted research on the time-spectrum variation patterns of epithermal and thermal neutrons under high count rates. In the software processing phase, a dead-time correction algorithm was incorporated to account for the effects of the pulse pileup. This algorithm converts the observed pileup count rate into a theoretical pulse count rate, thereby improving the uranium quantification accuracy during uranium logging [32].

3 Logging experiments

With the independently developed PFNUL instrument UNL4, a series of experiments was conducted in five standard model wells at the Nuclear Industry Airborne Survey and Remote Sensing Center. These wells consisted of cylindrical concrete models, identified as Nb4, Nu1, Nu2, and Nu3, with uranium concentrations of 0.000156%, 0.0280%, 0.0684%, and 0.0982%, respectively. The Nb4 model, with a uranium grade far below the detection limit, was defined as a pure sandstone model without uranium. Each cylindrical model was 1.4 m in diameter and 1.8 m in height. The borehole diameter of the models was 90 mm, and each model was topped with a 0.9 m-thick concrete cover and a 0.3 m-thick concrete base. Beneath the base, an extended borehole with a

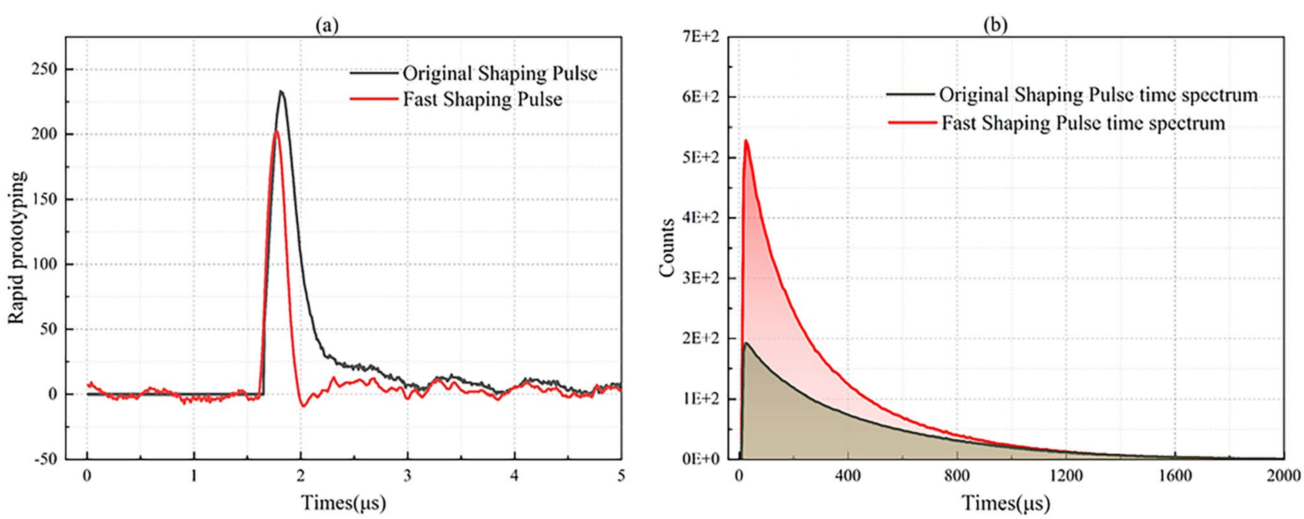

Fig. 5 (Color online) **a** Pulsed fast shaping measurement. **b** Neutron time-spectrum measurements in model wells before and after fast shaping

depth of 2.6 m ensured that the size requirements for the saturated uranium models were satisfied. Another logging model, identified as PU, was a single cylindrical concrete structure with dimensions of 1.5 m in diameter and 5.3 m in height, along with an extended layer of 3 m at the bottom. It contains two 90 cm sections with uranium contents of 87.1 ppm and 45.6 ppm, respectively. This setup allowed continuous measurement of the uranium section when logging within the PU model. Several experiments were conducted in these five model wells, as outlined below, including comparisons among different neutron tubes:

(1) Experiment #1: Neutron source comparison

This experiment compared the performance of a probe with the domestically developed FH-G5DT neutron tube and a probe with the Russian ING-10-20-120 neutron tube in four uranium models through point measurements.

(2) Experiment #2: Scale factor

Based on the time-spectrum data, the *E*/*T* values of both neutron tubes were calculated at different uranium concentrations. A scale factor for *E*/*T* values and uranium concentrations was derived by fitting.

(3) Experiment #3: Stability test

In this experiment, short-term measurements were repeated 10 times for 5 s each and long-term measurements were repeated nine times for 1 h each in the same uranium concentration model to assess stability.

(4) Experiment #4: Logging speed test

In the Nu3 model, neutron (*E*/*T* values) logging was conducted at speeds of 0.3, 0.5, 1, 1.5, 2, and 3 m/min to compare the results at different logging speeds, and gamma logging was conducted at speeds of 1, 2, 4, 6, 8, and 10 m/min.

4 Results and discussion

4.1 Comparison of different neutron sources

The time-spectrum results obtained by testing different neutron tubes using the four uranium ore models are shown in Fig. 6. Figure 6a shows the results of the assembly of the Russian ING-10-20-120 model neutron tube, whereas Fig. 6b shows the results for the FH-G5DT model neutron tube. Owing to variations in the neutron tube manufacturing processes, the pulse widths for the neutron tubes were appropriately set to 10 and 250 μs during the uranium ore measurements. The time-spectrum results indicated a significant proliferation of epithermal neutrons with increasing uranium ore content.

Figure 6 shows that the FH-G5DT neutron tube experiences a significant decline in the production of epithermal neutrons at approximately 250 μs, leading to a very low counting rate of epithermal neutrons for times greater than 850 μs. At this point, statistical fluctuations significantly affect the data, prompting the selection of 250 to 850 μs as the effective neutron time window. Similarly, the ING-10-20-120 neutron tube shows a significant decrease in epithermal neutron production at approximately 200 μs, with low counting rates exceeding 800 μs, where statistical fluctuations also play a significant role. Consequently, the effective neutron time window for this tube is defined as 200 to 800 μs. Within these time windows, the epithermal and

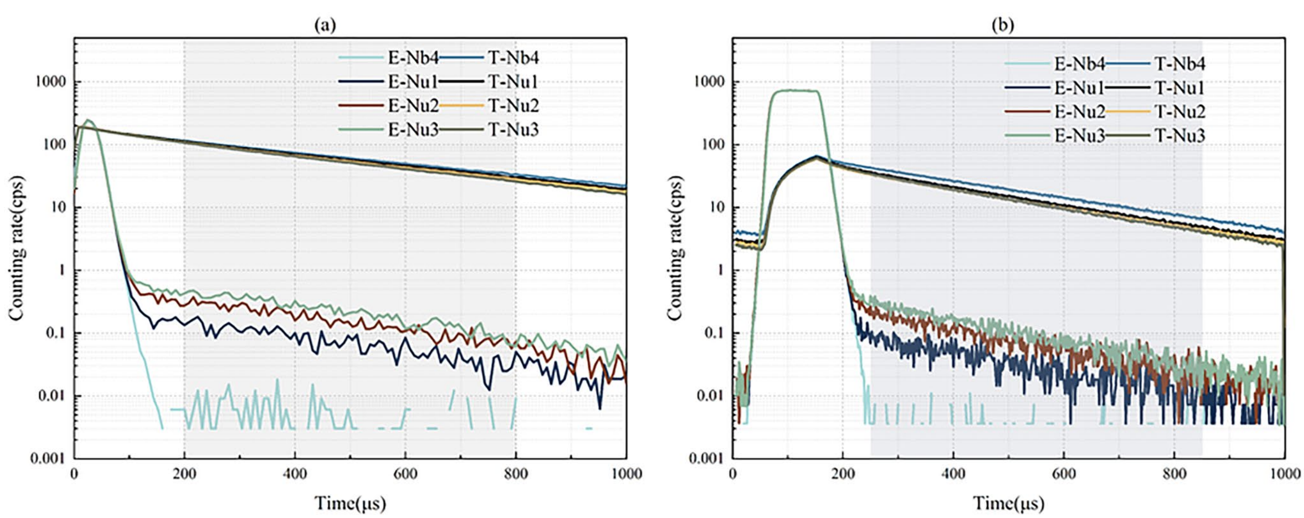

Fig. 6 (Color online) **a** ING-10-20-120 neutron tube time-spectra test results in Nu series model. **b** FH-G5DT neutron tube time spectra test results in Nu series model

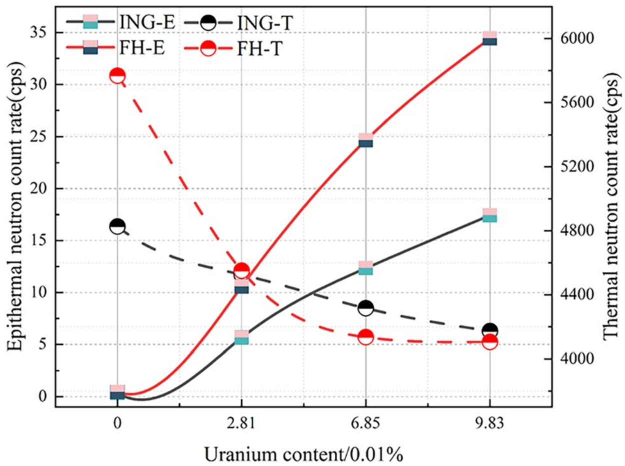

Fig. 7 (Color online) Epithermal and thermal neutron counting results for the ING-10-20-120 and FH-G5DT neutron tubes

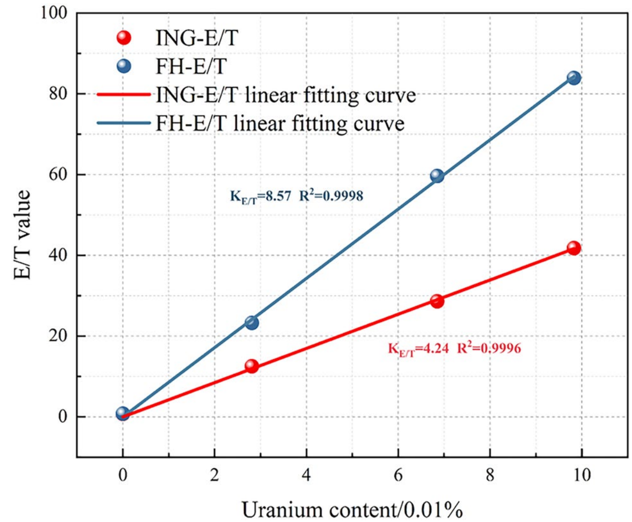

Fig. 8 (Color online) *E*/*T* scale curves ($K_{E/T}$) for ING-10-20-120 and FH-G5DT neutron tube

thermal neutron counts were calculated for various uranium content levels. The comparative results are shown in Fig. 7, revealing significant differences in the counting rates of epithermal and thermal neutrons between the two neutron tubes in the same model. These discrepancies are primarily attributed to the different ion sources employed by the two neutron tubes. The Russian ING-10-20-120 neutron tube utilizes a vacuum arc ion source that produces short pulses (1 μs) with a maximum of 20 emissions per second. In contrast, the FH-G5DT neutron tube, manufactured by Fan-Hua Testing Technology Co., employs a Penning ion source that generates longer pulses (150 μs) and can emit up to 1000 times per second.

4.2 Scale factor

Based on the aforementioned conditions, the uranium quantification time windows for the two neutron tubes are 200 ~ 800 μs and 250 ~ 850 μs, respectively. The *E*/*T* values were calculated based on relevant data. Subsequently, a linear fitting of the relationship between the *E*/*T* values and uranium content was performed, as shown in Fig. 8. Calibration curves for the FH-G5DT and ING-10-20-120 neutron tubes were obtained, with calibration coefficients of 8.57 and 4.24, respectively, and goodness-of-fit values (R^2) of 0.9998 and 0.9996, respectively. Both neutron-logging instruments demonstrated strong linear calibration for the standard uranium ore model, with R^2 values exceeding 0.999. The results indicate that the neutron source, which is a key component of a neutron-logging instrument, significantly influences the calibration coefficient. Therefore, the instrument should be recalibrated when the neutron source is changed using a standard model borehole.

4.3 Instrument stability

4.3.1 Short-term stability measurement

The UNL4 instrument was used for ten repeated measurements on the Nu3 model, using *RSD* as a metric to assess the instrument's stability, with the calculation formula shown in Eq. (1) [33, 34]. The results and *RSD* calculations are shown in Fig. 9a–c. Across the ten repeated measurements, the counts of thermal neutrons, epithermal neutrons, and *E*/*T* values exhibited good repeatability, with *RSD* values of 1.11%, 3.23%, and 3.16%, respectively.

$$RSD = \frac{\sqrt{\frac{\Sigma(count_i - \overline{count})^2}{n-1}}}{\overline{count}} \tag{1}$$

where $count_i$ represents the count for each dataset, $\overline{count}$ is the average count from multiple tests, *n* denotes the number of repeated measurements, and *RSD* is the relative standard deviation calculation used to assess instrument stability.

4.3.2 Long-term stability measurement

The UNL4 neutron-logging instrument was used to conduct nine 1-h long-term measurements on the Nu3 model. The data from each hour were normalized, and the parameters were selected based on the aforementioned time window. The effective thermal neutrons, epithermal neutrons, and *E*/*T* values within the time window were then calculated. The stability was analyzed using the *RSD* formula, with the specific data and calculation results shown in Fig. 9e and f.

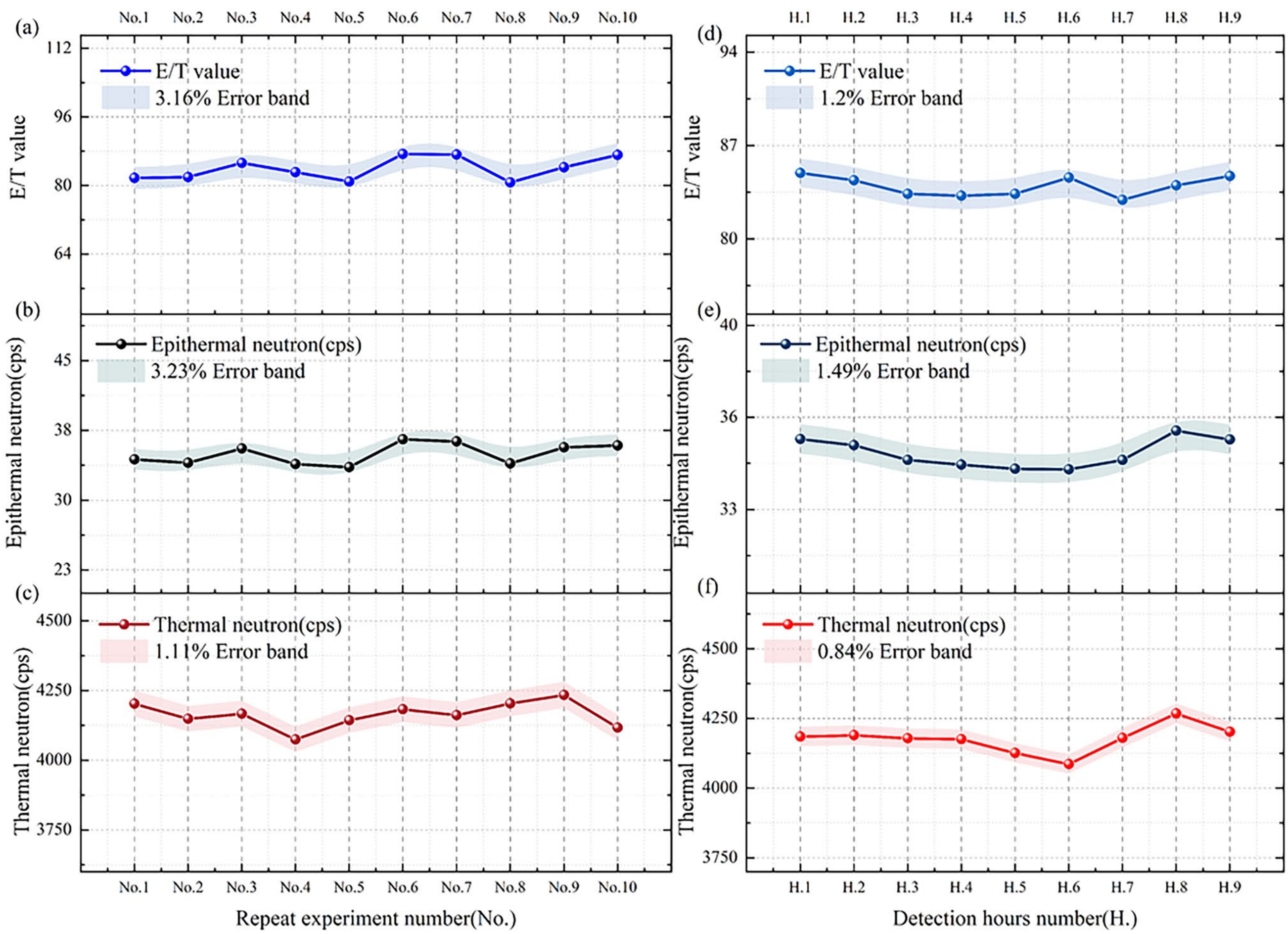

Fig. 9 (Color online) **a**–**c** Short-time measurements of *E*/*T* values, epithermal neutron counts rate, and thermal neutron counts stability for neutron detection systems. **d**–**f** Long-time measurements of *E*/*T* values, epithermal neutron counts rate, and thermal neutron counts rate stability for neutron detection systems

As illustrated in the figures, the long-term stability of the neutron detection system showed that the long-term stability of the thermal neutrons within the effective time window was 0.84%, that of epithermal neutrons was 1.49%, and that of the *E*/*T* values was 1.2%. These results demonstrated that the logging instrument exhibits excellent stability.

4.4 Experiments at different logging speeds

The UNL4 neutron-logging instrument was used to conduct measurements in the PU model well at the Remote Sensing Center, with neutron-logging speeds set to 0.3, 0.5, 1.0, 1.5, 2, and 3 m/min and gamma logging speeds set to 1, 2, 4, 6, 8, and 10 m/min. The neutron-logging curves obtained at these five speeds are shown in Fig. 10. At logging speeds ranging from 0.3 to 3 m/min, the uranium-bearing sections of the formation (red) could be accurately identified. The quantitative uranium curve (green) demonstrated consistency with the theoretical curve (red). Table 3 lists the relative errors (*RD*) of the quantitative values for the two uranium-bearing sections at different neutron-logging speeds. The formula for calculating *RD* is given by Eq. (2), where U_{Meas} represents the quantitative mean value of the ore section, and U_{Theor} is the theoretical value of uranium content. At logging speeds ranging from 0.3 to 3 m/min, *RD* was below approximately 10%. These findings indicated that the instrument can achieve stable quantification of uranium content at logging speeds of 0.3 to 3 m/min. A direct uranium content scale based on gamma counting was conducted for the gamma logging experiment at different logging speeds, and the results are shown in Fig. 11. The results of *RD* between the quantitative mean value and the theoretical values of the two ore sections are shown in Table 4, where *RD* was below about 10%, with good stability and accuracy.

$$RD = \frac{U_{\text{Meas}} - U_{\text{Theor}}}{U_{\text{Theor}}} \times 100\% \tag{2}$$

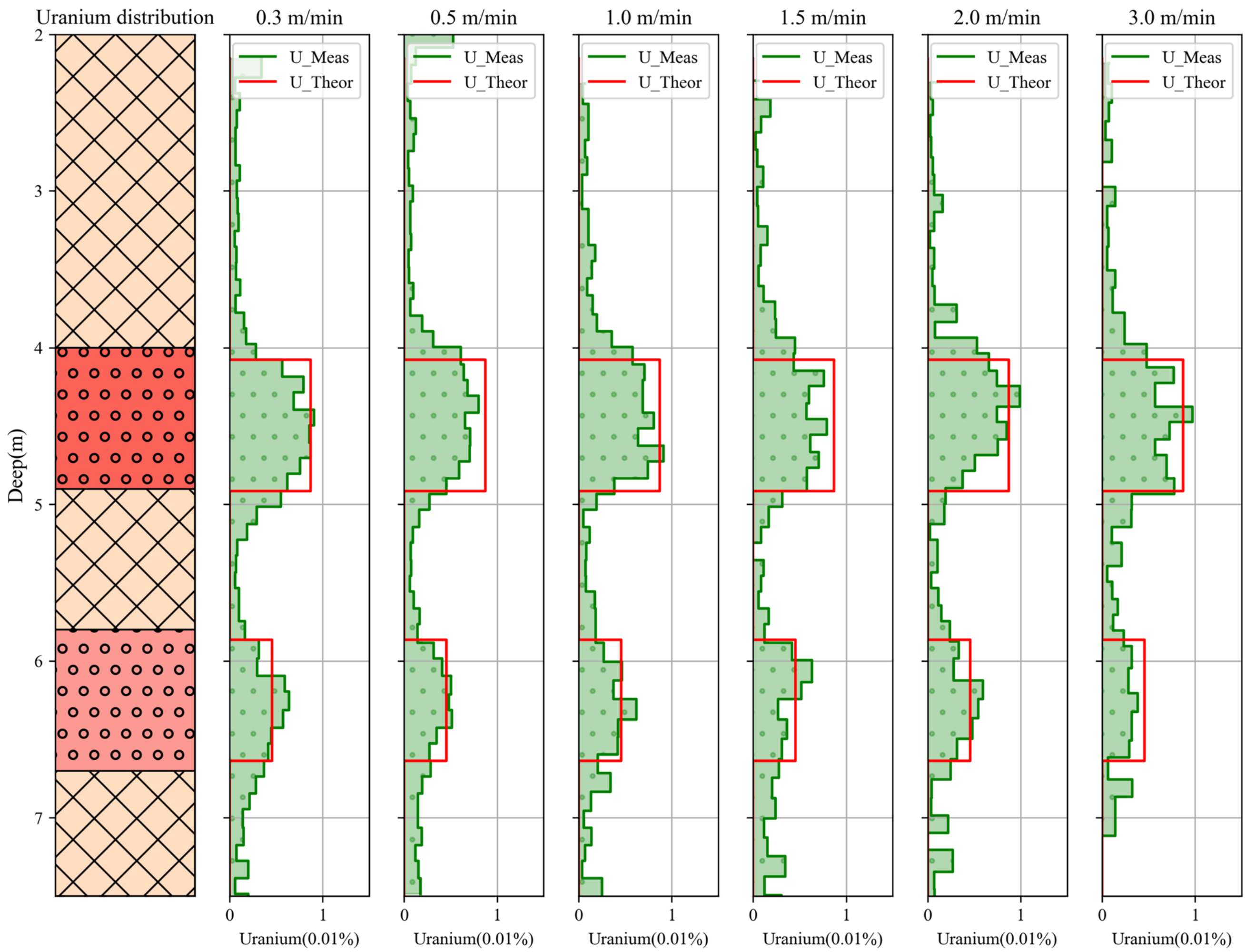

Fig. 10 (Color online) *E*/*T* values logging quantification curves of uranium content in PU model at logging speeds of 0.3, 0.5, 1.0, 1.5, 2, and 3 m/min

Table 3 Relative errors of uranium content *E*/*T* values scale at different logging speeds

Uranium content (ppm)		Neutron-logging speeds (m/min) 0.3	0.5	1.0	1.5	2.0	3.0
87.1	*RD*	−2.04%	0.81%	2.51%	−0.74%	0.70%	−10.45%
45.6		4.13%	−2.16%	12.55%	−4.91%	−0.66%	−20.37%

Table 4 Relative errors of uranium content gamma counts scale at different logging speeds

Uranium content (ppm)		Gamma logging speeds (m/min) 1.0	2.0	4.0	6.0	8.0	10.0
87.1	*RD*	3.35%	−0.99%	1.29%	−1.37%	4.55%	−7.42%
45.6		2.63%	9.38%	2.15%	4.40%	5.95%	5.80%

4.5 Instrument performance parameters

In summary, after a series of optimizations and related experiments, the instrument was proven to achieve international standards for key technical indicators. A detailed comparison of performance parameters is presented in Table 5 [35–37]. Owing to the use of the new pulse signal-shaping hardware design in this instrument, the neutron signal pulse width was

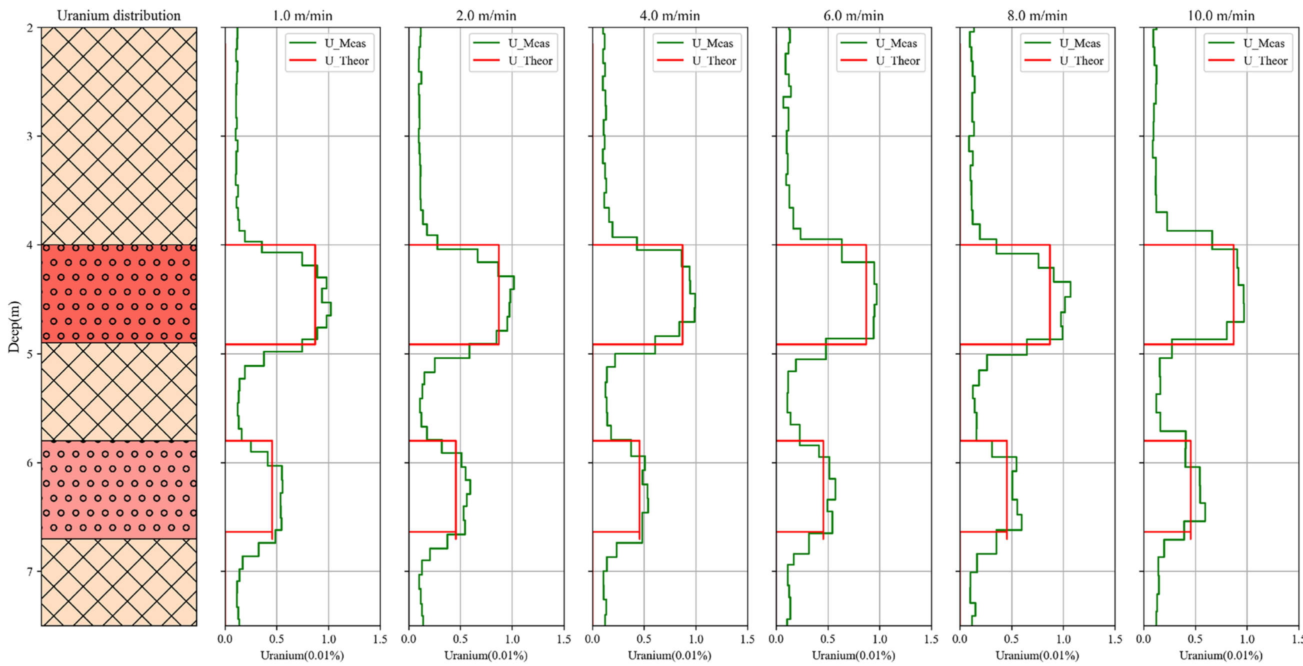

Fig. 11 (Color online) Gamma logging quantification curves of uranium content in PU model at logging speeds of 1, 2, 4, 6, 8, and 10 m/min logging speeds

Table 5 Comparison of key technical indicators

Parameter	USA (PFN) [35]	Australia (APFN$^+$) [36]	Russian (ANHK-60) [37]	Logging instrument UNL4 (this paper)
Thin-layer and formation resolution (cm)	15 (0.5 feet)	15 (0.5 feet)	–	10
Uranium detection limit (ppm)	500	50	50	45.6
Logging speed (orebody) (n/min)	0.5	1 (neutron) 6 (gamma)	0.6	3 (neutron) 10 (gamma)
Neutron tube life span (h)	–	–	150	≥ 250
Initial neutron tube output (n/s^{-1})	1×10^8	1×10^8	1.5×10^8	1.45×10^8
Pulsed neutron frequency (Hz)	100	1000	20	1000 (adjustable)
Detector type	^{3}He neutron detector (epithermal neutron) NaI gamma detector	^{3}He neutron detector (epithermal/thermal) $LaBr_3$ gamma detector	^{3}He neutron detector (epithermal) NaI gamma detector	^{3}He neutron detector (epithermal/thermal) $LaBr_3$ gamma detector

effectively reduced, thereby increasing the neutron detection efficiency. Coupled with a software dead-time correction algorithm [38], the time-spectrum acquisition accuracy was significantly improved, reducing the impact of dead time on uranium quantification. Additionally, the detector structure inside the probe was optimized, and a uranium quantification algorithm based on the ratio of thermal neutrons to epithermal neutrons was proposed [39]. This algorithm effectively reduces the impact of neutron source fluctuations, enabling accurate uranium content quantification. The neutron (*E*/*T* values) logging speed, gamma logging speed, and detection limit of the instrument have reached 3 m/min, 10 m/min, and 45.6 ppm, respectively. The operational life span of the instrument exceeded 250 h, and the neutron pulse width was adjusted as required. Compared with the other three instruments, this instrument demonstrated a significant performance improvement.

5 Conclusion

In this study, we developed a new uranium fission prompt neutron-logging instrument (UNL4), marking the first use of a domestically produced FH-G5DT neutron emitter, two ^{3}He proportional detectors, a lanthanum bromide ($LaBr_3$) gamma-ray detector, and a digital spectrometer. The system employs high-speed ADC and FPGA technologies to enable the rapid acquisition and transmission of dual-energy neutron time and gamma spectra. Additionally, a fast signal-shaping method was developed, which reduces the dead-time effect in ^{3}He detectors, thereby significantly improving the neutron signal detection efficiency. Monte Carlo simulations were used to optimize the thicknesses of Cd and HDPE for epithermal neutron detection. The optimal configuration was determined to be a Cd thickness of 1 mm and an HDPE thickness of 5 mm for the near ^{3}He detector, enabling the efficient detection of epithermal neutrons. The far ^{3}He detector was employed to detect thermal neutrons, whereas the $LaBr_3$ detector was used to detect gamma rays emitted by the uranium ore itself. Experimental results from standard borehole models with varying uranium content showed that the ratio of epithermal to thermal neutrons detected by instruments equipped with either the domestic FH-G5DT neutron tube or Russian ING neutron tube exhibited a strong linear relationship with uranium content, with R^2 values of 0.9998 and 0.9996, respectively. This validated the effectiveness of the newly developed uranium fission prompt neutron-logging instrument equipped with a domestic FH-G5DT neutron tube. Short-term testing indicated stability values of 1.11% for the thermal neutron count rate, 3.23% for the epithermal neutron count rate, and 3.16% for the E/T values, whereas long-term testing indicated stability values of 0.84% for the thermal neutron count rate, 1.49% for the epithermal neutron count rate, and 1.2% for the E/T values, confirming the high stability of the instrument. In addition, the instrument demonstrates good performance at neutron-logging speeds of $0.3 \sim 3\,\text{m/min}$ (E/T values) and gamma logging speeds of $1 \sim 10\,\text{m/min}$. By conducting measurements in two ore sections of the PU model with uranium contents of 87.1 ppm and 45.6 ppm, RD was found to be less than approximately 10% for different neutron and gamma logging speeds, and the detection limit reached 45.6 ppm. This instrument fills a critical gap in China's uranium exploration neutron-logging equipment and is of significant importance for the advancement of uranium exploration technology.

Author Contributions All authors contributed to the study conception and design. Material preparation, data collection and analysis were performed by Hai-Tao Wang, Yan Zhang, Chi Liu, Jian-Qiang Xu, Li-Jiao Zhang, Zhi-Feng Liu, Xiong-Jie Zhang, Rui Chen, Qi Liu, Ren-Bo Wang, Shu-Min Zhou, and Bin Tang. The first draft of the manuscript was written by Hai-Tao Wang and Yan Zhang, and all authors commented on previous versions of the manuscript. All authors read and approved the final manuscript.

Data Availability The data that support the findings of this study are openly available in Science Data Bank at https://cstr.cn/31253.11.sciencedb.14086 and https://doi.org/10.57760/sciencedb.14086.

Declarations

Conflict of interest The authors declare that they have no conflict of interest.

References

1. W. Xing, A. Wang, Q. Yan et al., A study of China's uranium resources security issues: based on analysis of China's nuclear power development trend. Ann. Nucl. Energy **110**, 1156–1164 (2017). https://doi.org/10.1016/j.anucene.2017.08.019
2. C.F. Mason, Uranium and nuclear power: the role of exploration information in framing public policy. Resour. Energy Econ. **36**(1), 49–63 (2014). https://doi.org/10.1016/j.reseneeco.2013.11.009
3. H.R. Zhang, Y. Zhang, W.X. Hu et al., Simulation study of uranium content in uranium yellow cake using the active multiplicity method. Nucl. Tech. (in Chinese) **47**(2), 020202 (2024). https://doi.org/10.11889/j.0253-3219.2024.hjs.47.020202
4. B. Hou, J. Keeling, Z.Y. Li, Paleovalley-related uranium deposits in Australia and China: a review of geological and exploration models and methods. Ore Geol. Rev. **88**, 201–234 (2017). https://doi.org/10.1016/j.oregeorev.2017.05.005
5. L.G. Howell, A. Frosch, Gamma-ray, well-logging. Geophysics **4**(2), 106–114 (1939). https://doi.org/10.1190/1.1440486
6. C. Lin, Y.Q. Chen, Q.W. Zhang et al., Calculation of U, Ra, Th and K contents in uranium ore by multiple linear regression method. Nucl. Tech. (in Chinese) **14**(6), 369–371 (1991). https://doi.org/10.0000/j.issn.1674-3849.1991.6.369371
7. B. Tang, Y.P. Wu, X.J. Zhang et al., Direct uranium quantitative detection in high precision γ-logging by 1.001 MeV ^{234m}Pa γ-ray. Nucl. Tech. (in Chinese) **35**(10), 745–750 (2012). https://doi.org/10.0000/j.issn.1674-3849.2012.10.745750
8. J.H. Renken, Determination of the probing distance in pulsed-neutron uranium logging experiments. Nucl. Sci. Eng. **63**(3), 330–335 (1977). https://doi.org/10.13182/NSE77-A27044
9. R.L. Caldwell, Nuclear logging methods. Radioisotopes **17**(4), 171–185 (1968). https://doi.org/10.3769/radioisotopes.17.4_171
10. W.W. Givens, W.R. Mills Jr., Logging technique for assaying for uranium in earth formations. U.S. Patent 4180730, 25 Dec 1979. https://www.osti.gov/biblio/5327390
11. Z.F. Liu, C.L. Ding, R.Y. Wang et al., Current status and development trend analysis of neutron logging in uranium mines in China. J. Phys. Conf. Ser. **1865**, 022006 (2021). https://doi.org/10.1088/1742-6596/1865/2/022006/meta
12. Y. Jin, F.L. Chen, X.Y. Chai et al., Development and application of nuclear logging technique. At. Energy Sci. Technol. **38**(S1), 201 (2004). https://doi.org/10.7538/yzk.2004.38.S1.0201
13. X.G. Wang, D. Liu, F. Zhang, Development of pulsed neutron uranium logging instrument. Rev. Sci. Instrum. **86**(3), 034501 (2015). https://doi.org/10.1063/1.4913660
14. C.P. Smith, P. Jeanneau, R.A.M. Maddeve et al., PFTNA logging tools and their contributions to in-situ elemental analysis of mineral boreholes. TOS forum **5**, 157–164 (2015). https://doi.org/10.1255/tosf.54
15. D. Chernikova, V.L. Romodanov, A.G. Belevitin et al., Experimental and numerical investigations of radiation characteristics of Russian portable/compact pulsed neutron generators: ING-031, ING-07, ING-06 and ING-10-20-120. Nucl. Instrum. Methods Phys. Res. Sect. A **746**, 74–86 (2014). https://doi.org/10.1016/j.nima.2014.01.061
16. K. Mikszuta-Michalik, R. Miklaszewski, Reconstruction of neutron spectrum emitted by portable 14 MeV neutron generator by a

combination of different methods. Fusion Eng. Des. **199**, 114129 (2024). https://doi.org/10.1016/j.fusengdes.2023.114129

17. D.W. Heikkinen, The rotating target neutron source II facility: operational summary. Nucl. Instrum. Methods Phys. Res. Sect. B **40–41**, 1162–1164 (1989). https://doi.org/10.1016/0168-583X(89)90562-4
18. J.H. Renken, Comparison of predicted signals from the delayed fission neutron and prompt fission neutron uranium logging methods. J. Appl. Phys. **49**(2), 6153–6159 (1978). https://doi.org/10.1063/1.324538
19. D.R. Humphreys, R.W. Barnard, H.M. Bivens et al. Uranium logging by the prompt fission neutron technique. IEEE Trans. Nucl. Sci. **28**, 1691–1695 (1981). https://doi.org/10.1109/TNS.1981.4331500
20. B. Tang, R.B. Wang, S.M. Zhou et al., Chinese Patent 201310408465.6, 13 Sept 2013. Chinese Patent 201310408465.6
21. B. Tang, R.B. Wang, S.M. Zhou et al., Chinese Patent 201320592725.5, 2 Apr 2014. Chinese Patent 201320592725.5
22. B. Tang, R.B. Wang, S.M. Zhou et al., Chinese Patent 201310440359.6, 13 Sept 2013. Chinese Patent 201310440359.6
23. Z.F. Liu, B. Tang, Z.H. Wei et al., Correction algorithm of epithermal neutron decay time spectrum for uranium pulsed neutron logging. For. Chem. Rev. 1368–1376 (2022). http://forestchemicalsreview.com/index.php/JFCR/article/view/804
24. X.G. Wang, D. Liu, G.B. Wang, Optimization study of epithermal neutron detector in prompt fission neutron uranium logging. Nucl. Tech. (in Chinese) **36**(6), 060401 (2013). https://doi.org/10.11889/j.0253-3219.2013.hjs.36.060401
25. H.Q. Zhang, B. Tang, H.X. Wu, Pulse amplitude extraction in digital nuclear spectrometer system. Nucl. Tech. (in Chinese) **36**(5), 050401 (2013) https://doi.org/10.11889/j.0253-3219.2013.hjs.36.050401
26. R. He, X.Y. Niu, Y. Wang et al., Advances in nuclear detection and readout techniques. Nucl. Sci. Tech. **34**, 205 (2024). https://doi.org/10.1007/s41365-023-01359-0
27. B. Tang, H.T. Wang, R. Cheng et al., Chinese Patent 201810076976.5, 6 Aug 2018. Chinese Patent 201810076976.5
28. D.W. Luo, H.Y. Wu, Z.H. Li et al., Performance of digital data acquisition system in gamma-ray spectroscopy. Nucl. Sci. Tech. **32**, 79 (2021). https://doi.org/10.1007/s41365-021-00917-8
29. C.H. Nowlin, Pulse shaping for nuclear pulse amplifiers. IEEE Trans. Nucl. Sci. **17**(1), 226–241 (1970). https://doi.org/10.1109/TNS.1970.4325584
30. D. Yan, G. Dai, Q. Yuan et al., Research and comparison of several common pulse forming algorithms. Open Access Library Journal **10**, e9847 (2023). https://doi.org/10.4236/oalib.1109847
31. V.T. Jordanov, G.F. Knoll, A.C. Huber et al., Digital techniques for real-time pulse shaping in radiation measurements. Nucl. Instrum. Methods Phys. Res. Sect. A. **353**(1), 261–264 (1994). https://doi.org/10.1016/0168-9002(94)91652-7
32. J.W. Müller, Dead-time problems. Nucl. Instrum. Methods **112**(1–2), 47–57 (1973). https://doi.org/10.1016/0029-554X(73)90773-8
33. Y. Zhang, B. Tang, W. Jia et al., Application of the Monte Carlo Library Least-Squares (MCLLS) approach for chromium quantitative analysis in aqueous solution. Appl. Radiat. Isotopes **150**, 39–42 (2019). https://doi.org/10.1016/j.apradiso.2019.02.018
34. Y. Zhang, W. Jia, R. Gardner et al., Study on the PGNAA measurement of heavy metals in aqueous solution by the Monte Carlo-Library Least-Squares (MCLLS) approach. Appl. Radiat. Isotopes **132**, 13–17 (2018). https://doi.org/10.1016/j.apradiso.2017.10.037
35. R.W. Barnard, W.A. Stephenson, J.H. Weinlein et al., Experiences with a PFN uranium logging system. IEEE Trans. Nucl. Sci. **30**(2), 1664–1667 (1983). https://doi.org/10.1109/TNS.1983.4332610
36. M. Horst, A.M. Smith, J. Ross et al., Advancements in exploration and in-Situ recovery of sedimentary-hosted uranium. In I*nternational Symposium on Uranium Raw Material for the IAEA - Nuclear Fuel Cycle: Exploration, Mining, Production, Supply and Demand, Economics and Environmental Issues*, Vienna, 2014. https://doi.org/10.13140/2.1.4322.2400
37. V.G. Martynenko, A.R. Minosyants, S.N. Fedyanin, The prospects for the application of the new generation neutron logging system developed by Rusburmash Inc (Russian Federation) for handling geotechnical issues at sandstone-hosted uranium deposits. *In International Symposium on Uranium Raw Material for the IAEA - Nuclear Fuel Cycle: Exploration, Mining, Production, Supply and Demand, Economics and Environmental Issues*, Vienna, 2014
38. Y. Zhang, C. Liu, S.L. Liu et al., Prompt fission neutron uranium logging (II): dead-time effect of neutron time spectrum. Nucl. Sci. Tech. **36**, 19 (2025). https://doi.org/10.1007/s41365-024-01615-x
39. Y. Zhang, C. Liu, H.T. Wang et al., Prompt fission neutron uranium logging (I): direct uranium quantification method theory. Nucl. Sci. Tech. **36**, 106 (2025). https://doi.org/10.1007/s41365-025-01691-7